# THERMAL ANALYSIS OF A CORELESS AXIAL FLUX PERMANENT MAGNET MACHINE

by

***Franjo PRANJIĆ*, Marko PEZDEVŠEK, and Peter VIRTIČ***

Faculty of Energy Technology, University of Maribor, Krško, Slovenia

Original scientific paper
https://doi.org/10.2298/TSCI220118086P

*The article deals with numerical analysis of a double sided coreless axial flux permanent magnet machine with two rotor disks and a coreless stator. Coreless stator represents copper windings which are held together by epoxy raisin, therefore a special focus has to be given to the stator temperature. In this article a numerical analysis is presented, which is based on the copper losses, namely the $I^2R$ product, where the resistance of the copper windings was both calculated as well as measured in the prototype machine.*

Key words: *axial flux, CFD, coreless, permanent magnet, temperature distribution*

## Introduction

Axial flux permanent magnet machines (AFPMM) are increasingly popular in the last decade due to their compactness and high degree of reliability and high-power density [1-7]. Different topologies are available, namely single sided (one stator and one rotor), double sided (single stator-double rotor or single rotor-double stator), and multistage (multiple rotors and stators). Selection of the topology depends on the application of the AFPMM [8].

This article deals with the coreless double sided topology with surface mounted permanent magnets (PM) on two external rotor disks. Advantages of this topology are absence of cogging torque [9] and use of a massive core of rotor disks instead of a laminated iron. Since there is no ferromagnetic core in the stator they can operate at a higher efficiency [10] compared to the conventional machines [11].

Torque and induced voltage sizes of this topology are mainly limited by outer dimensions of the machine (and its mass) as well as current density in the windings.

External dimensions of the machine limit the space for the installation of coils and PM and the maximum allowed temperature limits the current density in the windings [7, 12-14].

Since the temperature is a limiting factor for electrical machines the authors analyze it using different approaches. In [15] the literature review of the rotor-stator heat transfer in AFPMM as well as experimental techniques for convective heat transfer measurement are presented and in [16] an experimental method to measure the local heat flux inside an electrical machine by using sensors based on the transverse Seebeck effect in an AFPMM. In [17] a

*Corresponding author, e-mail: franjo.pranjic@um.si

cooling structure based on the geometry property and the assemble way of AFPMM is proposed and in [18] the cooling enhanced method with rectangular fins is introduced for improving the temperature distribution of rotor in AFPMM and verified by CFD simulation.

In this article a thermal analysis of a coreless axial flux PM machine is presented for the double sided coreless AFPMM which is based on the copper losses, calculated with the mean electrical current and the resistance of the winding. The article shows the importance of appropriate housing or a cooling method in order to avoid damage of the AFPMM, namely deformation of the stator.

The AFPMM used in the analysis was previously presented and optimised in [19].

## Methodology

The topology of the analyzed machine is relatively simple. It consists of two rotor disks with surface mounted PM and stator between those rotor disks. Figure 1 shows the structure of the machine [19].

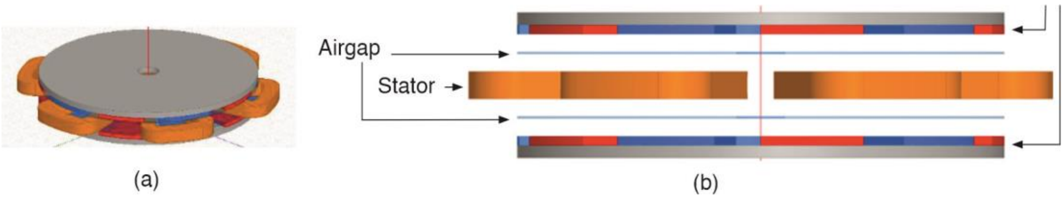


**Figure 1. Double-sided coreless AFPMM; (a) model and (b) components**

For a given design of AFPMM a thermal analysis was conducted for the thermal load, namely heat flux, determined in the electromagnetic analysis of the AFPMM (2408 W/m$^2$). It was calculated with the division of the copper losses of the machine, which were calculated using eq. (1) and the surfaces of all windings ($0.0208 \cdot 6 = 0.125$ m$^2$):

$$P_{\mathrm{Cu}} = 3I^2 R_{\mathrm{p}} \tag{1}$$

where $I$ is the nominal current of the AFPMM (20 A) and $R_{\mathrm{p}}$ measured ohmic resistance of one phase (0.25 Ω).

The prototype AFPMM is shown in fig. 2.

A steady-state simulation of the AFPMM was performed using ANSYS CFX 17.2, where the meshing was done with ICEM CFD 17.2. A block structured grid with approximately 14.3 million elements was made.

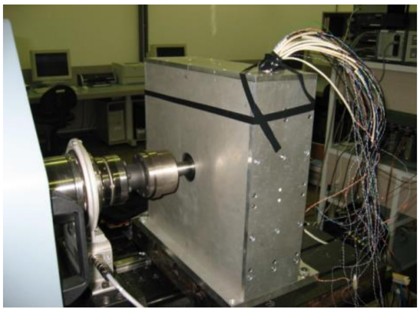

**Figure 2. Analyzed AFPMM**

### *Description of the analyzed machine (geometry, mesh, and boundary conditions)*

*Geometry*

The geometry was modeled in SolidWorks 2019. Each of the two rotor parts contain a rotor disk with 10 surface mounted PM. The stator part contains six coils. A cross-section of the electric motor with marked key parts is shown in fig. 3 and the basic geometry data in tab. 1.

The data shown in tab. 1 is also presented in the fig. 4, where on the left side the stator and on the right side the rotor is shown.

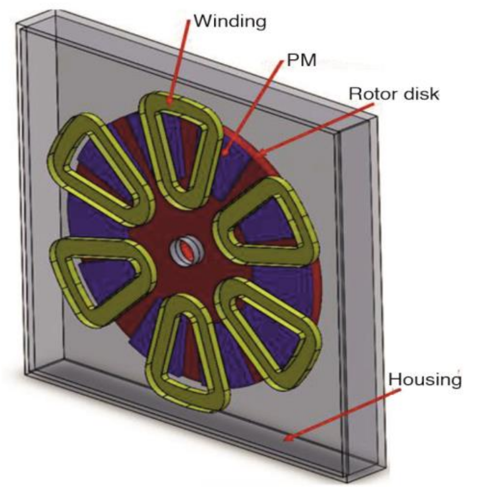


**Figure 3. Cross-section of the analyzed AFPMM**

**Table 1. Basic geometry data of the AFPMM [19]**

| Stator - housing | |
|---|---|
| Number of windings | 12 (2 × 6) |
| Coil width | 20 mm |
| Coil thickness | 15 mm |
| Coil span | 30° |
| Hight of the housing | 400 mm |
| Length of the housing | 400 mm |
| Thickness of the housing | 100 mm |
| Housing wall thickness | 5 mm |
| Rotor | |
| Rotor disk radius | 150 mm |
| Rotor disk thickness | 11.6 mm |
| PM thickness | 5 mm |
| PM span | 25° |
| PM inner radius | 80 mm |
| PM outer radius | 150 mm |
| Pole span | 36° |

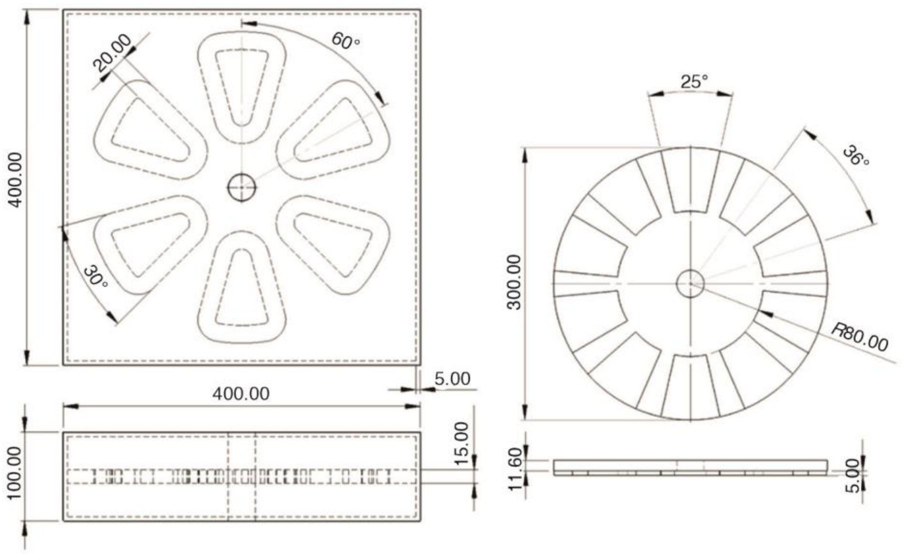


**Figure 4. Dimensions of the AFPMM**

*Mesh*

The mesh is divided into two domains, the rotor domain which contains the rotor parts (rotor disk, PM, and the surrounding air) and the stator domain which contains the stator parts (epoxy resin that holds together the windings, housing of the AFPMM, surrounding air, and the air within the AFPMM without the air in the proximity of the rotor).

Each component must be set as a separate body so the appropriate material and boundary conditions can be assigned. For both the stator and rotor parts a blocked structured mesh was created in ICEM CFD 17.2. Blocks of the stator and rotor parts are shown in fig. 5. It can be seen that half of the stator domain was meshed and the boundary condition symmetry was applied. For the rotor domain only one tenth of the domain was meshed and the boundary condition rotating periodicity was applied.

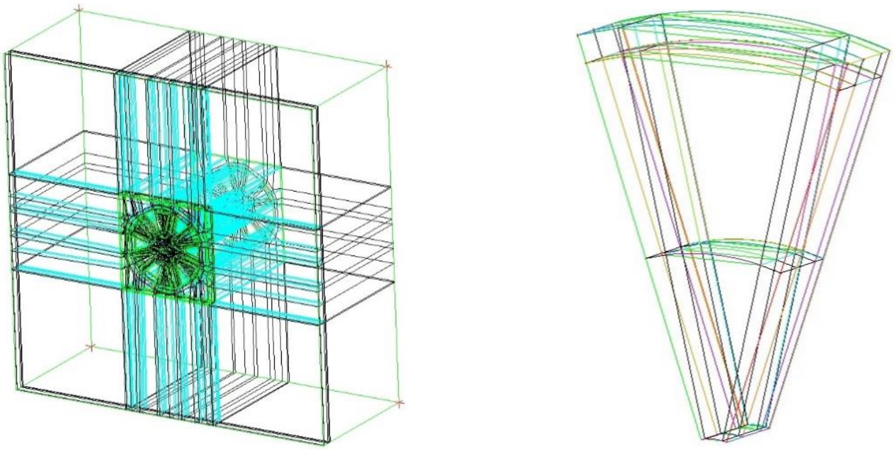

(a) (b)

**Figure 5. Meshed blocks of the stator and rotor parts; (a) stator parts and (b) rotor parts**

The final structured mesh of the stator parts is made out of 13.500.000 elements and it is shown in fig. 6.

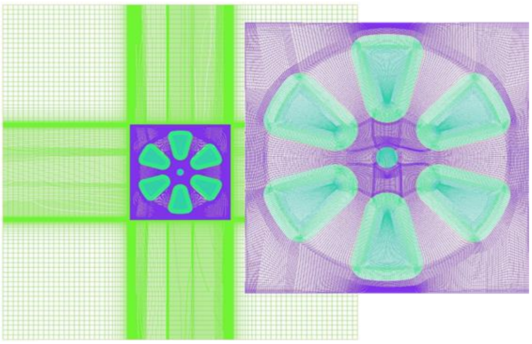

**Figure 6. Structured mesh of the stator parts**

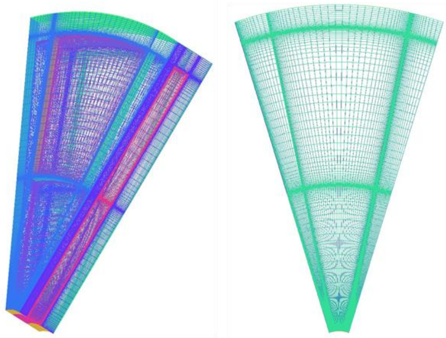

**Figure 7. Structured mesh of the rotor parts**

The final structured mesh of the rotor parts is made out of 800.000 elements and it is shown in fig. 7.

For the rotor and stator parts the goal was to reach the condition $y+ <= 1$. Based on the dimensionless number $y^+$ and eqs. (2)-(6) we calculated the distance from the wall of the first element [20].

Reynolds number is calculated:

$$\mathrm{Re} = \frac{\rho U_\infty L}{\mu} \tag{2}$$

where $\rho$ is the fluid density, $L$ – the characteristic length, $U_\infty$ – the free stream velocity, and $\mu$ – the dynamic viscosity of the fluid.

The skin friction coefficient for Reynolds numbers smaller than od $10^9$ is calculated by eq. (3) using the Schlichting aproximation solution:

$$C_f = \left[2\log_{10}\left(\mathrm{Re}\right) - 0.65\right]^{-2.3} \tag{3}$$

The wall shear stress is defined by eq. (4) and is calculated using the skin friction coefficient and the free stream velocity:

$$\tau_w = \frac{C_f \rho U_\infty{}^2}{2} \tag{4}$$

The friction velocity is defined eq. (5) and is calculated using the wall shear stress and the fluid density:

$$u_* = \sqrt{\frac{\tau_w}{\rho}} \tag{5}$$

The distance of the first element from the wall is defined by:

$$\Delta s = \frac{y^+ \mu}{\rho u_*} \tag{6}$$

### *Boundry conditions*

Boundary condition setting and stationary simulations were performed using ANSYS CFX 17.2. Within the program, we divided the model into the domains shown in tabs. 2-5 and figs. 8-11.

**Table 2. Domains of the PM and housing**

| Name of the domain | PM | Housing |
|---|---|---|
| Type of domain | Solid domain | Solid domain |
| Rotation | 1500 rev/min | No rotation |
| Material of the domain | Steel | Aluminum |
| Heat transfer | Thermal Energy | Thermal Energy |

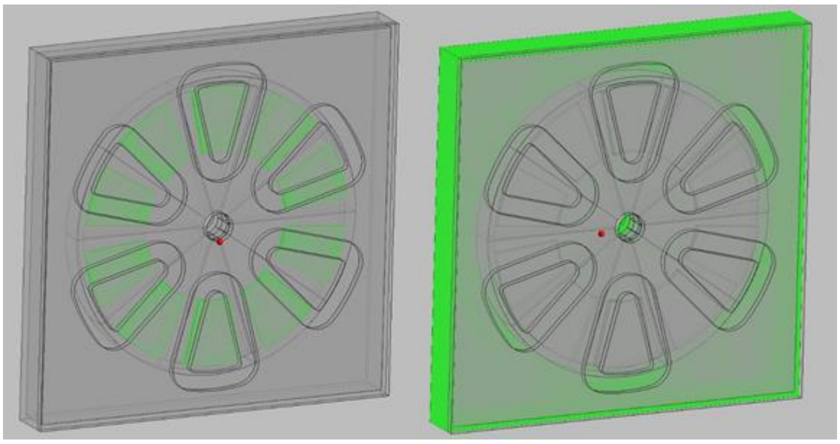

(a) (b)

**Figure 8. Domain of the PM (a) and housing (b)**

**Table 3. Domains of the epoxy resin and rotor disk**

| Name of the domain | Epoxy resin | Rotor disk |
|---|---|---|
| Type of domain | Solid domain | Solid domain |
| Rotation | No rotation | 1500 rev/min |
| Material of the domain | Epoxy raisin | Steel |
| Heat transfer | Thermal energy | Thermal energy |

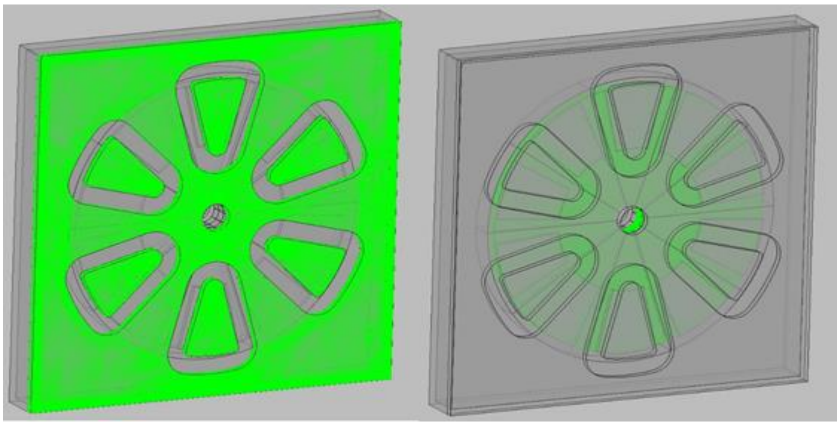

(a) (b)

**Figure 9. Domain of the epoxy resin (a) and rotor disk (b)**

**Table 4. Domains of the air around rotor and stator**

| Name of domain | Rotor air | Stator air |
|---|---|---|
| Type of domain | Fluid domain | Fluid domain |
| Rotation | 1500 rev/min | No rotation |
| Material of the domain | Air | Air |
| Heat transfer | Thermal Energy | Thermal Energy |
| Turbulent model | SST | SST |
| Buoyancy model | Non Buoyant | Non Buoyant |

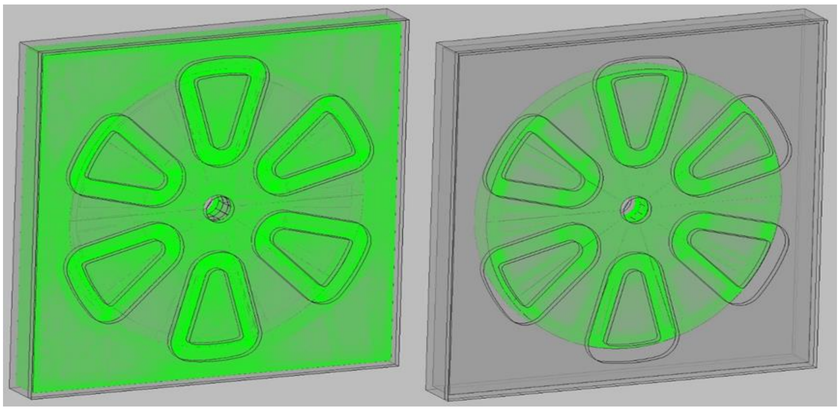

(a) (b)

**Figure 10. Domain of the air around rotor (a) and stator (b)**

**Table 5. Domain of the surrounding air**

| Name of the domain | Surrounding air |
|---|---|
| Type of domain | Fluid domain |
| Rotation | No rotation |
| Material of the domain | Air |
| Heat transfer | Thermal Energy |
| Turbulent model | SST |
| Buoyancy model | Buoyant - Temperature 300 K – Gravity in y direction 9.81 m/s$^2$ |

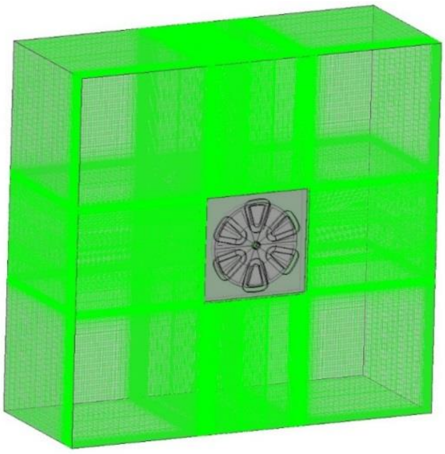

**Figure 11. Domain of the surrounding air**

For the upper, lower, rear, left, and right surfaces of the surrounding air the boundary condition opening was defined. The front surfaces of the surrounding air, housing, and epoxy resin domains were defined as symmetry. A heat flux of 2400 W/m$^2$ was defined on the surfaces of the windings, which was determined in a seperate magnetostatic analysis. The Frozen rotor condition was defined on the surfaces where the rotor and stator domains meet.

In the equation for conservation of momentum, the expression for the gravitational acceleration can be written:

$$\rho \mathrm{g} = \rho_0 \mathrm{g} + (\rho - \rho_0)\mathrm{g} = \nabla(\rho_0 \mathrm{g} \cdot \vec{r}) + (\rho - \rho_0)\mathrm{g}\frac{\partial \rho \vec{V}}{\partial t} + \nabla\left(\rho \vec{V} \otimes \vec{V}\right) = \nabla p' + (\rho - \rho_0)\mathrm{g} + \nabla \tau \tag{7}$$

In the domain of the surrounding air we acounted for natural convection and used the Boussinesq approximation, where the differences in density was ignored and the following eq. (8) is assumed:

$$\rho(T) - \rho_0 \approx \rho_0 \beta (T - T_0), \quad \beta(T - T_0) \ll 1 \tag{8}$$

The term $(\rho - \rho_0)$g can be eliminated for incompresible flow ($\rho = \rho_0$) and for compressible flow with modest density variations.

## Results

As mentioned in the previous section, the heat flux was calculated from copper losses, which were determined by using eq. (1) as well as measured. Table 6 shows the comparison of calculated and measured copper losses. It can be seen that the analyticaly calculated result is much smaller that the measured one.

**Table 6. Comparison of calculated and measured copper losses**

| | Analytical | Measured |
|---|---|---|
| Copper losses [W] | 300 | 423 |

While conducting the laboratory measurements of losses the measurements of temperatures of individual windings were also conducted. The temperature measurements were conducted using the measurement module FieldPoint, shown in fig. 12.

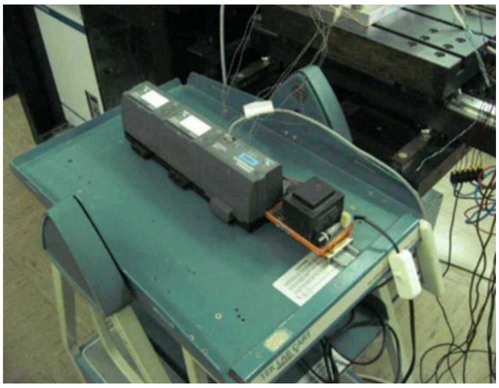

**Figure 12. Temperature measuring equipment**

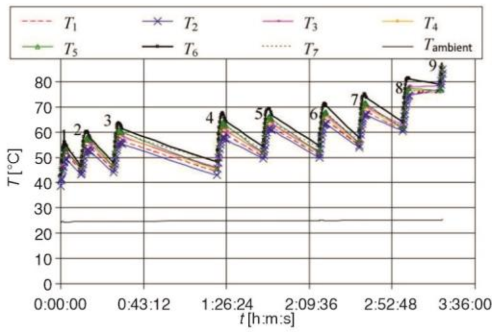


**Figure 13. Temperatures in individual windings**

Figure 13 shows the results of the temperature measurements.

Numbers from 1 to 9 in fig. 13 mark the sequence of the measurements at different rotation speed, namely as followed: 200, 400, 600, 800, 1000, 1200 rev/min, again 1000, 1500, and 1400 rev/min. Near the end of the measuring process we encountered a problem at rotation speed 1500 rev/min (and 1400 rev/min). the temperature reached the value at which the stator support structure started to deform, namely we heard the rotor touch the stator and finished the measuremet process. The result of rotor touching the stator can be seen on fig. 14 (red line at 15A) where the copper losses are shown.

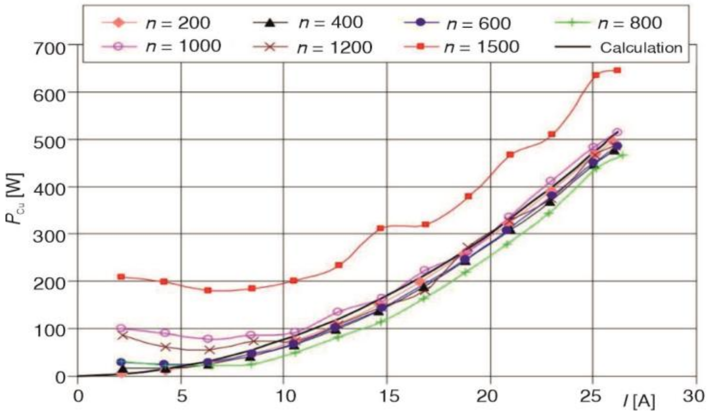


**Figure 14. Measured copper losses**

Due to the measuring problems we conducted the numerical thermal analysis. Even though the measured copper losses were higher than calculated losses, probably due to the deformation of the stator, we used the analytically obtained losses for the thermal analysis. The temperature distribution is shown in fig. 15. We can see that the highest temperature of 160 °C occurs at the source (winding). The maximum temperatures that occur on the surface of the windings are over the allowed limit, which is set by the epoxy resin manufacturer (maximum temperature should not exceed 150 °C).

Figure 16 shows the speed fields, from which we can see the speeds within the AFPMM are higher than 10 m/s while on the outer side, where the natural convection occurs, the speeds are significantly lower, around 0.6 m/s.

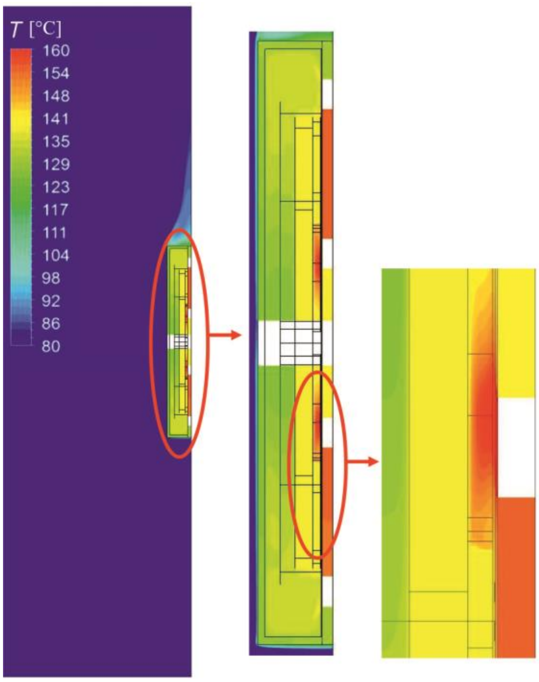


**Figure 15. Temperature distribution in AFPMM**

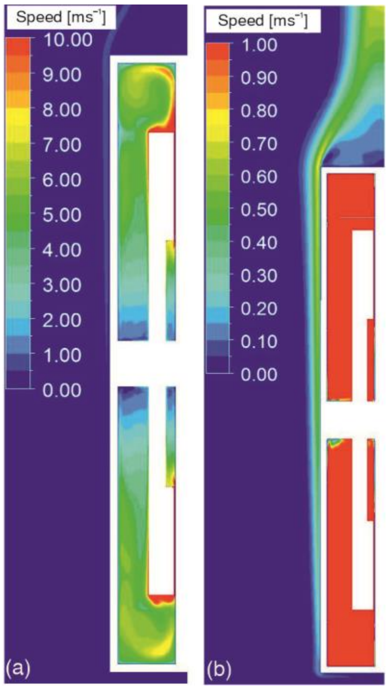


**Figure 16. Speed fields, (a) 0-10 m/s and (b) right 0-1 m/s**

## Conclusions

The article shows the importance of suitable cooling of the AFPMM, especially in the case of coreless topology. The analysis was performed for a prototype AFPMM with improvised housing, which is made out of aluminum plates, without any air inlet.

The obtained results are as expected, since the heat load applied was the value obtained from copper losses, namely 300 W divided by the surfaces of the windings. When the temperature was measured at constant 1500 rev/min the epoxy raisin, holding the windings in place, was slightly deformed. The main reason could be in the improvised housing of the machine without any air inlet or cooling.

The deformation itself cannot be shown, but its influence is shown in fig. 14 as the increase of copper losses at 1500 rev/min. The copper losses were in line with the calculated value for lower speed, even up to 1200 rev/min (around the calculated value 300 W). It can be assumed that the measured losses are higher at 1500 rpm due to the lack of cooling and consequently overheating of the stator.

It is clear that the improvised housing of the prototype AFPMM is not suitable, therefore ,in order to increase the heat dissipation it would be advisable to consider inlet and outlet slots that would help to supply cold air and exhaust warm air. In case the desired temperature is still not reached a forced convection should be considered with the help of a fan.

## Nomenclature

$P_{Cu}$ – copper losses, [W]
$I$ – nominal current, [A]
$R$p – phase resistance, [Ω]
Re – Reynolds number, [–]

$L$ – characteristic length, [m]
$U_\infty$ – free stream velocity, [m]
$C_f$ – skin friction coefficeint, [–]
$u_*$ – friction velocity, [ms$^{-1}$]
$\Delta s$ – distance of the first element from the wall, [m]
g – gravitational aceleration, [ms$^{-2}$]
$T$ – temperature, [K]
$T_0$ – operating temperature, [K]

*Greek symbols*

$\beta$ – thermal expansion coefficient, [K$^{-1}$]
$\rho$ – density, [kgm$^{-3}$]
$\rho_0$ – operating density, [kgm$^{-3}$]
$\mu$ – free stream velocity, [kg(ms)$^{-1}$]
$\tau_w$ – wall shear stress, [Pa]

## References


[1] Danang, W. F., *et al.*, Magnetic Flux Distribution Due to the Effect of Stator-Rotor Configuration in the Axial Machine, *Proceedings*, 6th Int. Conf. on Inf. Tec. And Electr. Eng., Yogyakarta, Indonesia, 2015
[2] Ekram, S., A Novel Windmill Generator, *Proceeding,s* 12th Int. Con. Ele. Mac. Sys., Tokyo, Japan, 2009
[3] Pop, A., *et al.*, Modeling and Permanent-Magnet Shape Optimization of an Axial-Flux Machine, *Proceedings*, 20th Int. Conf. Electr. Mach., Marseille, France, pp. 357-363, 2012
[4] Cao, Y., *et al.*, Rotor Mechanical Stress and Deformation Analysis of Coreless Stator Axial-Flux Permanent Magnet Machines, *Proceedings*, IEEE Magnetics Conference (INTERMAG), Beijing, China
[5] Wei, X., Yang, K., Research of Stator Displacement Technique in Multistage Axial-Flux Permanent Magnet Machines, *Proceedings*, IEEE Magnetics Conference (INTERMAG), Beijing, China, 2015
[6] Caricchi, F., *et al.*, Multistage Axial-Flux PM Machine for Wheel Direct Drive, *IEEE Trans. Ind. Appl., 32* (1996), 4, pp. 882-888
[7] Daghigh, A., *et al.*, Improved Design of Coreless Axial Flux Permanent Magnet Synchronous Generator with Low Active Material Cost, *Proceedings*, 6th Power Electronics, Drive Systems and Technologies Conference, Tehran, Iran, 2015, pp. 532-537
[8] Gieras, J. F., *et al.*, *Axial Flux Permanent Magnet Brushless Machines*, Kluwer Academic Publishers, Dordrecht, The Netherladns, 2004
[9] Virtic, P., *et al.*, Analytical Analysis of Magnetic Field and Back Electromotive Force Calculation of an Axial-Flux Permanent Magnet Synchronous Generator With Coreless Stator, *IEEE Trans. Magn., 44* (2008), 11, pp. 4333-4336
[10] Lombard, N., Kamper, M., Analysis and Performance of an Ironless Stator Axial Flux PM Machine, *IEEE Trans. Energy Convers., 14* (1999), 4, pp. 1051-1056
[11] Javadi, S., Mirsalim, M., A Coreless Axial-Flux Permanent-Magnet Generator for Automotive Applications, *IEEE Trans. Magn., 44* (2008), 12, pp. 4591-4598
[12] Chen, A., *et al.*, Performance Comparisons Among Radial Flux, Multi-Stage Axial Flux and Three-Phase Transverse Flux PM Machines for Downhole Applications, *Proceedings*, IEEE Int. Electr. Mach. Drives Conf., Miami, Fla., USA, pp. 1010-1017, 2009
[13] Hanselman, D. C., *Brushless Permanent Magnet Motor Design*, McGraw-Hill, New York, USA, 2003
[14] Howey, D. A., *et al.*, Air-Gap Convection in Rotating Electrical Machines, *IEEE Trans. Ind. Electron., 59* (2012), 3, pp. 1367-1375
[15] Howey, D. A., *et al.*, Measurement of Stator Heat Transfer in Air-Cooled Axial Flux Permanent Magnet Machines, *Proceedings*, IEEE Annu. Conf. 35th Ind. Electron., Porto, Portugal, 2009, pp. 1197-1202
[16] Jussila, H. K., *et al.*, Local Heat Flux Measurement in a Permanent Magnet Motor at No Load, *IEEE Transactions on Industrial Electronics, 60* (2013), 11, pp. 4852-4860
[17] Chai, F., *et al.*, Thermal Investigation and Cooling Enhancement of Axial Flux Permanent Magnet Motors for Vehicle Applications, *Proceedings*, 22nd Int. Con. on Ele. Mac. and Sys., Harbin, China, 2019
[18] Le, W., *et al.*, A Cooling Enhanced Method for Axial Flux Permanent Magnet Synchronous Machine, *Proceedings*, IEEE Int. Con. on App. Superconductivity and Electromagnetic Dev., Tianjin, China, 2020
[19] Pranjić, F., Virtič, P., Designing Rotor Disks of a Coreless Axial Flux Permanent Magnet Machines by Using Simplified FEM and an Approximation Method, *IEEE Transactions on Energy Conversion, 35* (2020), 3, pp. 1505-1512
[20] ***, CFD Online, https://www.cfd-online.com/Wiki/Y_plus_wall_distance_estimation


Paper submitted: January 18, 2022
Paper revised: February 6, 2022
Paper accepted: March 8, 2022